research paper

Acta Cryst B STRUCTURAL SCIENCE CRYSTAL ENGINEERING MATERIALS

ISSN 2052-5206

New insights into the structural properties of κ-(BEDT-TTF)$_2$Ag$_2$(CN)$_3$ spin liquid

Pascale Foury-Leylekian,[a]* Vita Ilakovac,[b,c] Pierre Fertey,[d] Victor Baledent,[a] Ognjen Milat,[e] Kazuya Miyagawa,[f] Kazushi Kanoda,[f] Takaaki Hiramatsu,[g] Yukihiro Yoshida,[g,h] Gunzi Saito,[g,i] Pere Alemany,[j] Enric Canadell,[k] Silvia Tomic[e] and Jean-Paul Pouget[a]

[a]Université Paris-Saclay, CNRS, Laboratoire de Physique des Solides, 91405, Orsay, France, [b]Sorbonne University, UPMC, LCP-MR, CNRS UMR 7614, Paris, F-75252, France, [c]Department of Physics, Cergy-Pontoise University, Cergy-Pontoise, F-95031, France, [d]Synchrotron SOLEIL, L'Orme des Merisiers, Saint-Aubin, BP 48, Gif-sur-Yvette, F-91192, France, [e]Institute of Physics, Bijenička cesta 46, Zagreb, HR-10000, Croatia, [f]Department of Applied Physics, University of Tokyo, Tokyo, 113-8656, Japan, [g]Faculty of Agriculture, Meijo University, Nagoya, 468-8502, Japan, [h]Division of Chemistry, Graduate School of Science, Kyoto University, Kyoto, 606-8502, Japan, [i]Toyota Physical and Chemical Research Institute, Nagakute, 480-1192, Japan, [j]Departament de Ciència de Materials i Química Física and Institut de Química Teòrica i Computacional (IQTCUB), Universitat de Barcelona, Martí i Franquès 1, Barcelona, 08028, Spain, and [k]Institut de Ciència de Materials de Barcelona (ICMAB-CSIC), Campus de la UAB, Bellaterra, 08193, Spain.
*Correspondence e-mail: pascale.foury@u-psud.fr

Received 11 December 2019
Accepted 20 April 2020

Edited by J. Lipkowski, Polish Academy of Sciences, Poland

Keywords: Mott transition; molecular spin liquids; geometrical frustration; X-ray diffraction.

Supporting information: this article has supporting information at journals.iucr.org/b

Here, the first accurate study is presented of the room-temperature and 100 K structures of one of the first organic spin liquids, κ-(BEDT-TTF)$_2$Ag$_2$(CN)$_3$. It is shown that the monoclinic structure determined previously is only the average one. It is shown that the exact structure presents triclinic symmetry with two non-equivalent dimers in the unit cell. But surprisingly this does not lead to a sizeable charge disproportionation between dimers. The difference from the analogue compound κ-(BEDT-TTF)$_2$Cu$_2$(CN)$_3$ which also presents a spin liquid phase is discussed in detail. The data provided here show the importance of the anionic layer and in particular the transition metal position in the process of symmetry breaking. The possible impact of the symmetry breaking, albeit weak, on the spin-liquid mechanism and the influence of various disorders on the physical properties of this system is also discussed.

1. Introduction

Magnetism and superconductivity are manifestations of two different ordered states which are generally mutually exclusive (Matsubara *et al.*, 1984). The interplay between these states is one of the richest subjects of investigation in condensed matter science. In this context, Mott insulators with strong magnetic interactions and in close proximity to an unconventional superconducting phase are intensively studied. The effect of the proximity of the magnetic ground state, usually antiferromagnetic (AFM), is an essential ingredient to understand the origin of superconductivity. An interesting situation occurs in the case of spin frustration as observed in the κ-(BEDT-TTF)$_2X_2$(CN)$_3$ (BEDT-TTF or ET is bis(ethylenedithio)tetrathiafulvalene and X = Ag and Cu) series (Powell & McKenzie, 2011; Balents, 2010; Komatsu *et al.*, 1996) and expected to lead to a quantum spin liquid. The quantum spin liquid (QSL) ground state is predicted for localized $S = \frac{1}{2}$ spins antiferromagnetically coupled on a perfect triangular lattice. Its experimental realization is strongly challenging but seems to have been observed in κ-(BEDT-TTF)$_2X_2$(CN)$_3$ (X = Cu, Ag). The influence of the lattice degrees of freedom on the mechanism of stabilization of such a ground state is of tremendous importance. Indeed, a

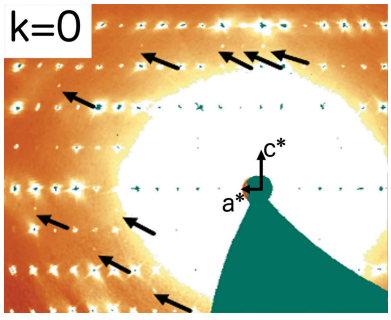

structural modification can reduce the magnetic frustration required in the QSL while a disorder can favour it (Watanabe *et al.*, 2014)

The charge transfer salts κ-(BEDT-TTF)$_2X_2$(CN)$_3$ (M = Cu and Ag) (Shimizu *et al.*, 2003, 2016), hereafter named κ-ET-Cu and κ-ET-Ag, are systems in which strong electronic correlations ($U/W \simeq 1$ where U is the onsite Coulomb coupling and W the bandwidth) lead to a Mott insulating phase (Jeschke *et al.*, 2012; Kandpal *et al.*, 2009; Koretsune & Hotta, 2014; Hiramatsu *et al.*, 2017; Pustogow *et al.*, 2018). These systems are two-dimensional compounds consisting of the stacking of molecular layers of ET dimers on a triangular lattice. Each dimer carries one hole and thus one $S = \frac{1}{2}$ spin, so that the triangular arrangement of spins is magnetically frustrated. The magnetic frustration is strong as J/J' is close to unity for both compounds, as showed by the ratio between transverse integrals along the two triangular paths: $t'/t \simeq 0.97$ for κ-ET-Ag and $t'/t \simeq 0.83$ for κ-ET-Cu (Shimizu *et al.*, 2016; Jeschke *et al.*, 2012; Kandpal *et al.*, 2009; Nakamura *et al.*, 2009). Although no QSL is theoretically expected for a triangular lattice of $S = \frac{1}{2}$ spins (Bernu *et al.*, 1992), the 3D low-temperature phases of κ-ET-Cu and κ-ET-Ag behave as a QSL (Kanoda & Kato, 2011). They are characterized by the absence of long-range magnetic order at low temperature in spite of the strong magnitude of the exchange interactions (J_{Cu} = 250 K and J_{Ag} = 175 K) (Shimizu *et al.*, 2003; Shimizu *et al.*, 2016). QSL behaviour is assessed by the temperature dependence of the T_1 NMR relaxation time which presents a power-law behaviour (Shimizu, Miyagawa *et al.*, 2003). In addition, the heat capacity has a linear evolution as a function of the temperature as expected for a QSL (Shimizu *et al.*, 2016, Yamashita *et al.*, 2008). Finally, a broad mode below 600 cm^{-1} is observed in Raman spectra and attributed to low-lying magnetic excitations characteristic of a QSL (Nakamura *et al.*, 2017, 2014). Regarding the features pointed out above, κ-ET-Cu and κ-ET-Ag are now considered as the first organic QSLs.

The pressure-temperature phase diagram of these salts is very rich. Indeed, a thermodynamic phase transition around 6 K, with significant lattice and sound velocity (Manna *et al.*, 2010; Poirier *et al.*, 2014) anomalies, is observed in κ-ET-Cu. Importantly, a recent resonant inelastic X-ray scattering study of κ-ET-Cu has been able to probe the vibration spectra of nitrogen atoms from the anion layer sizably coupled to the ET molecules and to measure the electron-phonon coupling (Ilakovac *et al.*, 2017). Under a moderate pressure of less than 4 and 10 kbar in κ-ET-Cu and in κ-ET-Ag, respectively, the metallic character is recovered and a superconducting ground state is observed (Shimizu *et al.*, 2016; Kurosaki *et al.*, 2005). Thus, the replacement of Cu by Ag acting as a negative chemical pressure enabled the study of a QSL in κ-ET-Ag in a very wide pressure range.

In addition, these salts present unusual dielectric properties at low temperatures which could play a major role in the establishment of the QSL via a spin-dipolar coupling (Watanabe *et al.*, 2014; Naka & Ishihara, 2010, 2013; Gomi *et al.*, 2010; Gomi *et al.*, 2013, 2016; Hotta, 2010). Indeed, both κ-ET-Cu and κ-ET-Ag, present a frequency-dependent dielectric anomaly at around 20 K, characteristic of a relaxor behaviour (Abdel-Jawad *et al.*, 2010; Pinterić *et al.*, 2014, 2016). However, no charge disproportionation is detected by optical measurements (Nakamura *et al.*, 2017; Pinterić *et al.*, 2016, 2018; Sedlmeier *et al.*, 2012). Thus, a detailed investigation of structural properties is of great interest to understand the dielectric properties as a signature of ferroelectric fluctuations.

Previous studies reported that κ-ET-X with M = Cu and Ag crystallize in the non-polar mean $P2_1/c$ structure (Shimizu *et al.*, 2016; Geiser *et al.*, 1991; Bu *et al.*, 1997; Yamochi *et al.*, 1992; Papavassiliou *et al.*, 1993). The structure consists of (**b**,**c**) layers of strongly dimerized ET molecules, with each dimer oriented approximately perpendicular to its nearest neighbours. The two molecules of the dimer, as well as the two dimers of the unit cell, are symmetry equivalent in the $P2_1/c$ space group. The ET layers alternate along the **a** direction with non-conductive $[M_2(CN)_3]^-$ anionic layers. The poly-

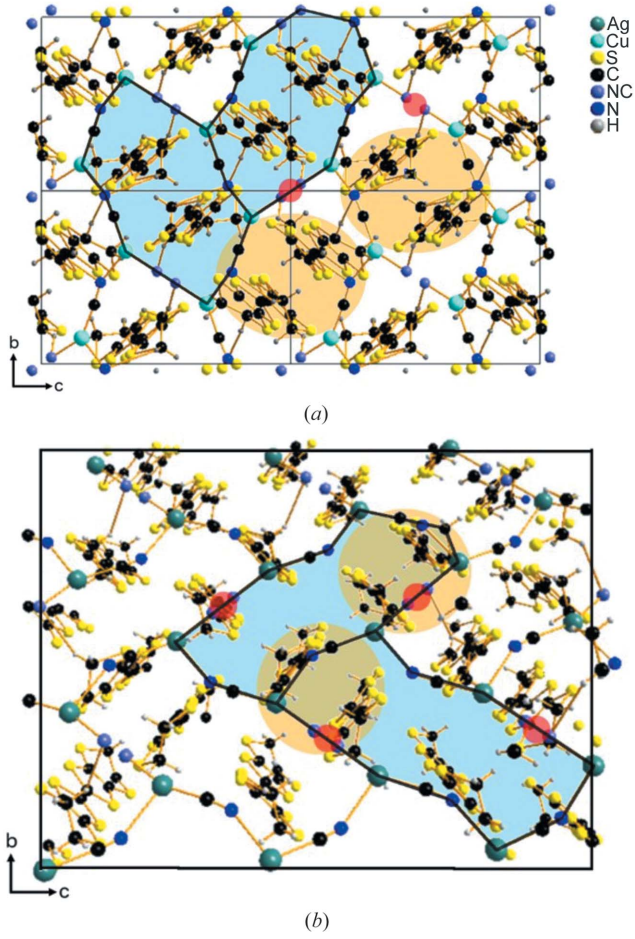

Figure 1
View of the (**b**,**c**) anionic layer of κ-ET-M. Note that the openings in the anionic plane of (*a*) κ-ET-Cu and (*b*) κ-ET-Ag do not have the same shape. The dimers of molecules (orange circles) are positioned in front of the openings (blue cavities) formed by the anionic layer for κ-ET-Cu while, they are located in front of the cyanide groups for κ-ET-Ag. The red circles represent the inversion centres located on the disordered CN groups.

meric-like anionic layer is composed of *M*CN chains, running along the **b** axis, connected by (bridging) cyanide (CN) groups. These groups are located on the centre of inversion of the structure. This automatically induces a disorder of occupation on the C and N sites. Another type of disorder, generally observed in other ET salts, has its origin in the molecular layer. The disorder at 300 K corresponds to the occurrence of various configurations of the C_2H_4 group (staggered, S or eclipsed, E) (Pouget *et al.*, 2018). An ordering of ethylene groups is frequently observed upon cooling [a recent review on that topic is given by Pouget *et al.* (2018)]. The connection between the molecular and anionic layer is different for κ-ET-Cu and κ-ET-Ag because of the different shape of the openings in the anionic layers of the two salts (Fig. 1) (Hiramatsu *et al.*, 2017).

In order to better understand the puzzling properties of these salts, the crystallographic structure of κ-ET-Cu was recently reinvestigated (Foury-Leylekian *et al.*, 2018). In this work, we obtained the exact structure which crystallizes in the $P\bar{1}$ space group and is given as CCDC 1825317 in the Cambridge Structural Database (Groom *et al.*, 2016) with lattice parameters a = 16.1221 (10) Å, b = 8.591 (6) Å, c = 13.412 (8) Å, α = 89.99 (2)°, β = 113.43 (2)° and γ = 90.01 (2)°. This result means that two dimers in the unit cell are non-equivalent, while the two molecules within each dimer remain equivalent. In the structure obtained, we have a fractional occupancy of 72% and 28%, for the S and E conformations of the ethylene molecule respectively close to those given by Geiser *et al.* (1991), Hiramatsu *et al.* (2015). In addition, we observed a twist conformation on each side of the molecule (the S and E conformations, as well as the twist and half-twist ethylene configurations are defined by Pouget *et al.* (2018) [see also Fig. 2 given by Foury-Leylekian *et al.* (2018)]. Finally, by analysing the hydrogen bonds between the ethylene groups and the electronegative (N or C) atoms of the anionic stack, we observed that the interaction with the anionic network does not clearly favour one of the two conformations of the ET molecule. This explains the observed disorder between the E and S conformations. Most importantly, from the crystal structure we obtained the charge of the ET molecules using an analysis described by Guionneau *et al.* (1997). We showed a charge disproportionation of 0.06±0.02 between the two dimers of ET molecules. This disproportionation was calculated to be much smaller via DFT calculations (0.01) (Foury-Leylekian *et al.*, 2018).

For κ-ET-Ag, no recent investigation of the structure was performed. The purpose of this paper is to present the accurate study of its structure as well as its thermal evolution. We also aim at comparing the main features of κ-ET-Cu and κ-ET-Ag. Finally, we discuss how our result impacts the physical properties of κ-ET-Ag.

2. Materials and methods

High-quality single crystals of κ-ET-Ag were synthesized by electro-crystallization following the process used in Hiramatsu *et al.* (2017). Crystals appear as thin plate-like samples with a surface of less than 1 mm^2 and a thickness of less than 1 mm corresponding to the (**b**,**c**) plane. We have performed preliminary X-ray diffraction measurements using a Cu $K\alpha$ radiation laboratory source and a homemade three-circle diffractometer equipped with a pulse tube cryo-generator. The full data collection has been performed on the synchrotron radiation facility SOLEIL at the CRISTAL beamline using a Newport four-circle diffractometer equipped with a Rigaku Oxford Diffraction Atlas CCD detector at a wavelength of 0.6717 Å. About 20 000 reflections were collected. Data were processed using the *CrysAlis Pro* suite (Rigaku Oxford Diffraction, 2015). The structure was solved *ab initio* using the charge flipping algorithm (*Superflip* sotftware). The obtained structure did not contain the H atoms. Missing H atoms were introduced by hand in the refinement program in a way that the C—N—H_2 groups form a tetrahedron. The *ab initio* structure was then refined using full-matrix least squares with *Jana2006* software (Petricek *et al.*, 2014). All non-hydrogen atoms were refined with anisotropic displacement parameters.

First-principles calculations were carried out using a density functional theory (DFT) approach (Hohenberg *et al.*, 1964; Kohn *et al.*, 1965), which was developed for efficient calculations in large systems and implemented in the *SIESTA* code (http://departments.icmab.es/leem/siesta/, accessed 25 February 2020; Artacho *et al.*, 2008). We used the generalized gradient approximation (GGA) to DFT and, in particular, the functional of Perdew, Burke and Ernzerhof (Perdew *et al.*, 1996). Only the valence electrons are considered in the calculation, with the core being replaced by norm-conserving scalar relativistic pseudopotentials (Troullier & Martins, 1991) factorized in the Kleinman–Bylander form (Kleinman *et al.*, 1982). We have used a split-valence double-ζ basis set including polarization orbitals with an energy shift of 10 meV for all atoms (Artacho *et al.*, 1999). The energy cut-off of the

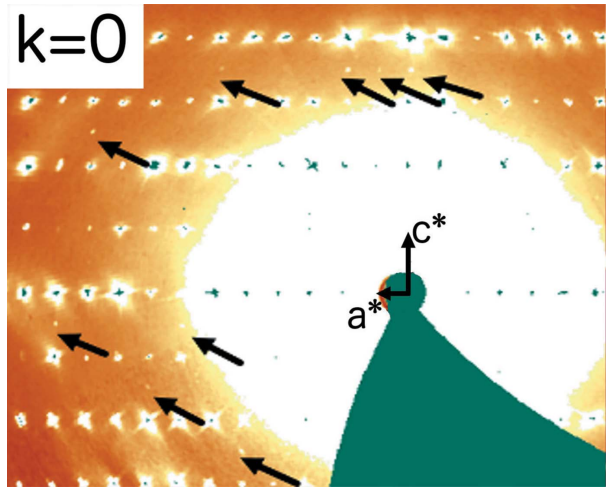

Figure 2
Reconstruction of the (**a***, **c***) reciprocal plane taking into account the absorption correction. The thinner arrows indicate the directions of the reciprocal lattice parameters, and the thicker arrows show the reflections forbidden in the $P2_1/c$ space group which are related to the breaking of the **c** glide plane.

real space integration mesh was 350 Ry. The Brillouin zone was sampled using a grid of (5 × 20 × 20) *k*-points (Monkhorst *et al.*, 1976). The room-temperature crystal structure as well as the 100 K structure of κ-ET-Ag were used for the calculations.

3. Results

3.1. Evidence for $P2_1/c$ symmetry breaking

To check the symmetry of the structure of the κ-ET-Ag salts, we used our laboratory X-ray measurements as well as synchrotron experiments and investigated specific reciprocal planes. Indeed, the non-symmorphic symmetry elements of the $P2_1/c$ group imply that in the $h0l$ reciprocal planes (for the glide plane **c**), Bragg reflections with an odd l value, are forbidden. As for the 2_1 screw axis, the Bragg reflections of the $0k0$ type with an odd value of k, are forbidden. We have measured several samples. For all the samples, except for one which was very small and had a very weak diffracted signal, we have observed the systematic presence of these forbidden reflections (see Fig. 2). It is important to indicate that the forbidden reflections are observed even at high scattering angles. Thus, they do not originate from a thermal effect, nor from a disorder, but rather from atomic displacements. We can also notice that the breaking of the 2_1 screw axis is attested by the presence of only two reflections (050 and 070) due to the intrinsically small number of reflections of the $0k0$ type.

We have excluded all possible experimental artefacts able to produce the forbidden reflections. The possibility of multiple scattering has been ruled out due to the systematic character of the detected reflections. We also excluded the possibility of a twinning because no symmetry operation can lead to the observed forbidden reflections particularly at low Bragg angle. We thus concluded that the new structural effect is an intrinsic characteristic of the compound. This conclusion is further supported by experimental arguments.

First, we have studied the profile of the reflections. We have observed that their width corresponds to the experimental resolution. In addition, we have not detected any diffuse scattering. We can thus conclude that the forbidden reflections are not due to disorder or stacking faults.

Second, we have measured the intensity of these forbidden reflections. They are systematically weaker than those allowed for $P2_1/c$ authorized ones. Taking into account the difference of scales between the two datasets, the ratio between the average of their intensity and the mean intensity of the standard Bragg reflections is 4×10^{-2}. This is one order of magnitude larger than for κ-ET-Cu (Foury-Leylekian *et al.*, 2018). The weakness of the forbidden reflections explains why they were not detected in previous automatic data collections. The difference of intensity with the κ-ET-Cu is an indication that the transition metal contributes to the intensity of these forbidden reflections (the X-ray scattering factor of Cu being smaller than that of Ag).

The existence of the various forbidden reflections of the $P2_1/c$ space group is the fingerprint of a symmetry breaking from the average structure associated with this space group to a real structure whose space group is a sub-group of $P2_1/c$, compatible with our observations. Regarding the absence of existence conditions for the forbidden reflections detected and the possible sub-group of $P2_1/c$ proposed in the Bilbao server (Gallego *et al.*, 2012), there are only two possible symmetries for the real structure: $P1$ and $P\bar{1}$. Notice that the deviation of the unit-cell parameters from a monoclinic symmetry is very small because the α and γ angles are close to 90° (see Section 3.2). Within the two possible space groups $P1$ is polar and compatible with the ferroelectricity. However, using standard diffraction experiments, we are not able to distinguish between the two space groups.

3.2. Structure

For our refinements we used the $P\bar{1}$ space group as the lack of inversion symmetry leading to $P1$ could not be detected. We followed the same procedure used in reference (Foury-Leylekian *et al.*, 2018). We directly obtained good reliability factors with correct thermal factors for all the atoms including those of the ethylene groups. Fig. 3 represents a view along the b axis of the refined structure. Fig. 4(*a*) shows displacement ellipsoids for one of the two molecules. In order to improve the quality of the refinement and ADPs as well as to check a possible disorder between E and S configurations, we introduced a splitting of the ethylene group as we did for κ-ET-Cu. However, this modelling did not improve the refinement. This shows that the ethylene groups are ordered (Shimizu *et al.*, 2003; Hiramatsu *et al.*, 2017). The configuration we obtained

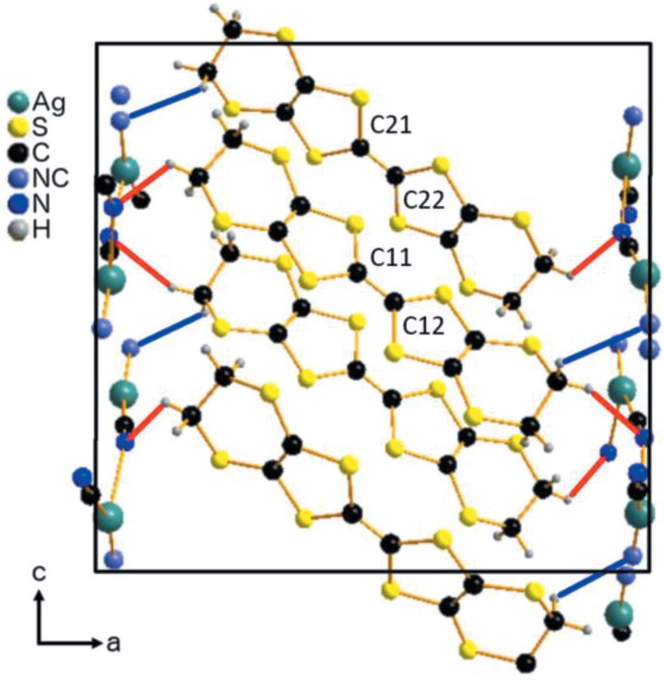

Figure 3
Structure of κ-ET-Ag at 300 K viewed along the **b**-axis. The shortest hydrogen bonds between the ethylene groups and the N atom of the ordered CN groups are represented by red lines. The longer hydrogen bonds with the disordered N/C atoms are shown in blue.

for them is the half-twist eclipsed configuration presented in Fig. 4(*b*).

The best refinement of the structure at 300 K in the $P\bar{1}$ space group is given in the CCDC 1971108 file. The refinement led to $R = 0.047$, $wR = 0.0656$, with $N = 11\,624$ reflections [9 054 with $I > 3\sigma(I)$] for a total of 397 refined parameters, 34 constraints, and two restraints. The lattice parameters are a = 15.0831 (3) Å, b = 8.64470 (10) Å, c = 13.4755 (3) Å, α = 90.012 (2)°, β = 91.364 (2)° and γ = 89.9980 (10)°. One can notice that the deviation from the monoclinic symmetry are larger than the error bars: for α the deviation corresponds to 6σ and for γ to 2σ.

The nearly flat shape of the core of the ET molecules as well as the central Ci1–Ci2 distances of the two dimers (Table 1) are in agreement with those expected for a $+\frac{1}{2}$ charged molecule and obtained for other κ-ET compounds (Bu *et al.*, 1997; Yamochi *et al.*, 1992; Papavassiliou *et al.*, 1993). We compared the refined atomic positions with those of reference (Hiramatsu *et al.*, 2017) obtained with the average $P2_1/c$ space group. Both structures are similar and the difference is at most of 0.01 ± 0.001 Å for the flat part of the ET. A stronger difference (0.07 ± 0.001 Å) is observed for the C atoms of the ethylene groups as well as for the ordered N atoms of the anionic layer. It is interesting to notice that the transition metal Ag also endures a slight displacement of about 0.01 ± 0.001 Å compared to the average $P2_1/c$ structure. This displacement is roughly twice that of the Cu atoms deduced from our refinement (0.006 ± 0.001 Å). The ratio between the forbidden reflections intensity measured for κ-ET-Ag and κ-ET-Cu (Foury-Leylekian *et al.*, 2018) (which is about 10) scales with the ratio between the square of the Ag and Cu scattering factors (2.6) times the square of the ratio of the Ag and Cu atomic displacements (2.8). This is what is expected if the reflections arise primarily from the displacement of the metal atoms. It shows the importance of the anionic layer and in particular the transition metal position in the symmetry breaking process.

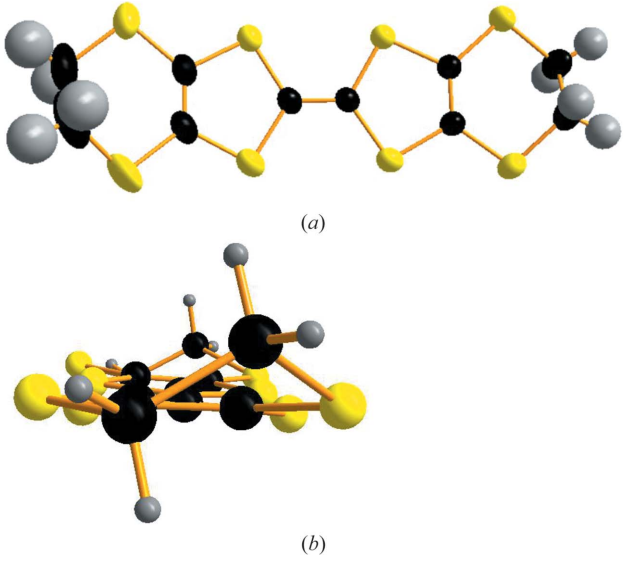

(*a*)

(*b*)

Figure 4
(*a*) ET molecule in the κ-ET-Ag with corresponding displacement ellipsoids at 300 K. Note that the displacement ellipsoids are larger on one side of the molecule. (*b*) Representation of the two terminal ethylene groups (without the displacement ellipsoids) which are in the half-twist eclipsed configuration. The eclipsed configuration corresponds to C atoms nearly symmetric with respect to a plane orthogonal to the central C═C bond of the ET molecule. The half-twist conformation means that only half of the C atoms of the C_2H_4 groups are out of the plane of the molecule.

Interestingly, the concomitant displacements of the ordered cyanide groups and of the ethylene group induce short hydrogen bonds between the N and H atoms: 2.58 and 2.65 Å for dimer 1 and 2.61 and 2.63 Å for dimer 2. These hydrogen bonds are shorter by 0.1 Å when compared to the hydrogen bonds in κ-ET-Cu (Foury-Leylekian *et al.*, 2018). Other longer hydrogen bonds are present with the disordered CN group: 2.84 Å for dimer 1 and 2.87 Å for dimer 2. The role of these short hydrogen bonds in the ordering of the ethylene group will be discussed in detail in Section 4.

We performed a similar measurement at 100 K. The result of the refinement is given in the CCDC files. The results give $R = 0.0451$, $wR = 0.0734$ for a total of 397 refined parameters, 34 constraints, and two restraints. The lattice parameters are a = 15.0062 (3) Å, b = 8.58200 (10) Å, c = 13.3243 (3) Å, α = 89.984 (2)°, β = 91.447 (2)°, and γ = 90.0020 (10)°. One can notice that the deviation from monoclinic symmetry is larger than the error bars: for α the deviation corresponds to 8σ and for gamma to 2σ. The structure is very similar to that obtained at 300 K. In particular, the shape of the molecule is not strongly modified. The comparison between the structures at 300 K and 100 K shows an average variation of atomic positions of 0.05 Å. This corresponds to standard thermal contractions. The major atomic displacements come from the C atom of the ordered cyanide group as well as from the peripheral sulfur atoms of the ET molecule. This indicates that the connection between the molecular and the anionic layers through hydrogen bonds is slightly modified by the temperature. At 100 K we find that the hydrogen bonds become 2.55 and 2.62 Å for dimer 1 and 2.54 and 2.61 Å for dimer 2. The longer hydrogen bonds with the disordered group are now 2.87 Å for dimer 1 and 2.88 Å for dimer 2. Thus, except for the expected slight increase in the hydrogen-bond strength when lowering the temperature, the only remarkable observation is that the two dimers become even more similar at 100 K.

4. Discussion

4.1. Difference between the two salts

The main difference between the structure of κ-ET-Cu and κ-ET-Ag concerns the order of the terminal ethylene groups of the ET molecules. In the case of κ-ET-Cu these groups are disordered between the S and E configurations while for the κ-ET-Ag they are ordered in an eclipsed half-twist configuration. The origin of this structural difference necessarily comes from the anionic layer, its shape and the way it connects with the molecular layer. Concerning the connection between the ET and the anionic layer, we remark that very short hydrogen

bonds are established with the N atoms of the ordered cyanide groups for κ-ET-Ag (2.58–2.61 Å) while in κ-ET-Cu the hydrogen bonds are longer (2.68 – 2.69 Å). These hydrogen bonds, which are considerably shorter in the κ-ET-Ag salt, are probably responsible of the absence of disorder in the κ-ET-Ag structure. We believe that this is ultimately related to the shape of the anionic layer. The rectangular openings present in the κ-ET-Ag anionic layer, even if they have a smaller surface (Hiramatsu *et al.*, 2017), give more freedom to the ET molecules to establish stronger interaction with the anion layer, as proven by the fact that the donor molecules are less densely packed in the κ-ET-Ag salt (Koretsune & Hotta, 2014). As a consequence of the different shape of the anionic plane opening, in the κ-ET-Cu salt the donors are more constrained when trying to optimize the hydrogen bond based interaction with the anion layer resulting with two disordered different conformations. Note in that case that the interaction with the disordered CN group, which is less effective for the hydrogen-bond stabilization, is somewhat stronger than for κ-ET-Ag. In other words, since the shape of the anionic layer does not allow the ethylene groups of ET to optimize the interaction with the ordered CN groups, the system tries to recover part of the hydrogen-bond stabilization through the interaction with the less effective disordered CN group. This is an additional factor which favours the ET disorder. It is however interesting to notice that the conformation is half twist in κ-ET-Ag which is not the one of lowest energy for the isolated molecule. This indicates anyway that the environment of the ET molecule should constrain the ethylene conformation. Other examples of how the competition of different hydrogen bond-based interactions influence the ET conformation are given by Pouget *et al.* (2018).

4.2. Inter/intra-dimer charge disproportionation?

The observation of a symmetry breaking from the previously accepted $P2_1/c$ space group to $P\bar{1}$ (or $P1$) should have consequences on the physical properties of these salts. In particular, it has an impact on the dielectric behaviour. Indeed, within the $P\bar{1}$ symmetry, the two dimers present in the unit cell are no longer symmetry equivalent. This leads to two different intra-dimer distances d for dimer 1 and dimer 2. In principle, d should be shorter for the more charged dimer. The distances in Table 1 are very similar suggesting a very weak charge disproportionation. A measure of how much the ET charge departs from the ideal one (*i.e.* δ) can be evaluated using the relationship of Guionneau *et al.* (1997). Using the crystal structures at 300 K we obtain the values +0.49 for the ET molecule in dimer 1 and +0.51 in dimer 2 (see Table 1) leading to a smaller charge disproportionation ($2\delta = 0.02 \pm 0.02$) than for κ-ET-Cu [$2\delta = 0.06 \pm 0.02$; Foury-Leylekian *et al.*, 2018).

To put these results on a firmer basis, we have also carried out first-principles DFT calculations. Because of the disorder of the CN anion bridging groups, we carried out two different types of calculation. In the first calculation, the original $P\bar{1}$ structure has been converted into a $P1$ structure by selecting one of the two possible orientations of the CN pair at the inversion centre but leaving the rest of the structure unaltered. In the second calculation, the anionic layer is completely removed and the neutrality of the system is enforced using a uniform background of charge amounting to two electrons per unit cell. In that way, the $P\bar{1}$ original symmetry is kept. The density of holes per ET donor was calculated by integration of the density of states of the two upper HOMO bands and the two calculations led to the same charges.

Table 1
Relevant interatomic distances (Å) for the structure of κ-ET-Ag at 300 and 100 K.

Intra-dimer distance d (d_1 and d_2 for dimer 1 and 2) denotes the distance between the core carbons of the two molecules of a given dimer. The charge disproportionation 2δ is defined as the difference between charges on dimer 1 and on dimer 2. Values of 2δ obtained from the structural correlation (Guionneau *et al.*, 1997) as well as from DFT calculations are also given. Dimer 2 is slightly more positively charged.

	300 K	100 K
d_1	3.782 (3)	3.718 (1)
d_2	3.785 (3)	3.7211 (10)
C11—C12 dimer 1	1.371 (3)	1.3646 (10)
C21—C22 dimer 2	1.362 (3)	1.368 (1)
2δ (structural correlation)	0.02±0.02	0.01±0.02
2δ (DFT)	< 0.01	< 0.01
H···N dimer 1	2.58, 2.65	2.55, 2.62
H···N dimer 2	2.61, 2.63	2.54, 2.61
H···CN dimer 1	2.84	2.875
H···CN dimer 2	2.87	2.878

The calculated band structure for the 300 K structure of κ-ET-Ag is shown in Fig. 5(*a*). The two upper bands are built from the anti-bonding combination of the two highest occupied molecular orbitals (HOMO) of the ET dimers. The two bands nearly merge all together along the *Z*–*M* and *M*–*Y* lines (there is complete degeneracy for the $P2_1/c$ space group). As it can be seen the separation between these two bands along the *Z*–*M* and *M*–*Y* lines is quite small (between 1 and 5 meV). As this separation is proportional to the difference between the two types of dimers (*i.e.* the difference in energy of the HOMOs anti-bonding combination of each dimer and the difference in transfer integrals between dimers of the same type along **b**), one must conclude that the intra- and inter-donor interactions for both types of dimers must be very similar. This is confirmed by the fact that the DFT electronic structure dispersion of Fig. 5 is nearly identical to that of the $P2_1/c$ structure (Jeschke *et al.*, 2012). In addition, the partial densities of states associated with the two different dimers practically superpose in Fig. 5(*b*). Note that according to model calculations, even a small charge disproportionation (2δ) of 0.06 leads to a very clear separation of the two bands and significantly different partial densities of states. As expected from these results, despite the existence of the two different dimers, the holes are calculated to be practically equally shared by the two dimers ($2\delta \cong 0.01$ for κ-ET-Cu and even smaller for κ-ET-Ag). The results of vibrational spectroscopy (Pinterić *et al.*, 2016, 2018; Sedlmeier *et al.*, 2012), which reveal a charge imbalance too small to reveal a true

charge order, are consistent with the present results despite the existence of two different dimers. Furthermore, we did not find any relevant difference between the DFT calculations at 300 K and 100 K. Use of the structural relationship by Guionneau *et al.* (1997) also led to practically the same value of the ET charges for the two temperatures.

The charge disproportionation calculated by DFT even if small leads to a pattern of charge-rich and charge-poor dimers as represented in Fig. 6. This should lead to a pattern of electric dipoles. These dipoles are however weak because the charge disproportionation between dimers is small. The origin of the charge disproportionation is complex. It can be due to strong inter-site Coulomb repulsions. The low-temperature charge ordered ground state observed in several families of $(BEDT\text{-}TTF)_2X$ salts (Alemany *et al.*, 2012, 2015; Seo *et al.*, 2006) is usually due to these interactions. However, in charge ordered compounds, the charge order is expected to increase with decreasing temperature (Tomić & Dressel, 2015; de Souza *et al.*, 2009). This is not the case in κ-ET-Ag salts according to our results. A difference of environment of the ET dimers and the strong hydrogen bonds with the anionic stack can more likely be at the origin of the charge disproportionation, as observed in several families of $(BEDT\text{-}TTF)_2X$ salts (Pouget *et al.*, 2018; Alemany *et al.*, 2012, 2015; Seo *et al.*, 2006).

As mentioned previously, our X-ray measurements cannot totally exclude the absence of a centre of inversion in the structure. If the space group is $P1$ rather than $P\bar{1}$, the scenario may be more complex. Indeed, with the two ET molecules of a dimer being no longer equivalent, an intra-dimer charge disproportionation can occur. The presence of such intra-dimer electric dipoles, if of non-zero value, would have a strong impact on the dielectric properties which reveal a relaxor behaviour (Abdel-Jawad *et al.*, 2010; Pinterić *et al.*, 2014, 2016, 2018). The presence of such dipoles is also assumed to have an impact on the spin-liquid state via a dipolar-spin model based on a strong coupling analysis (Tomić & Dressel, 2015); Hotta (2010); Li *et al.* (2010). Unfortunately, our X-ray diffraction experiments are not able to disentangle the presence or the absence of an inversion centre in the structure of these salts. Second harmonic generation (SHG) is a useful experiment to check the presence of a centre of inversion. But SHG has been attempted without success in κ-ET-Cu probably because the system is too conducting. THz electric field pump–SHG probe measurements also do not succeed to show a permanent and stable charge order (Miyamoto, 2019).

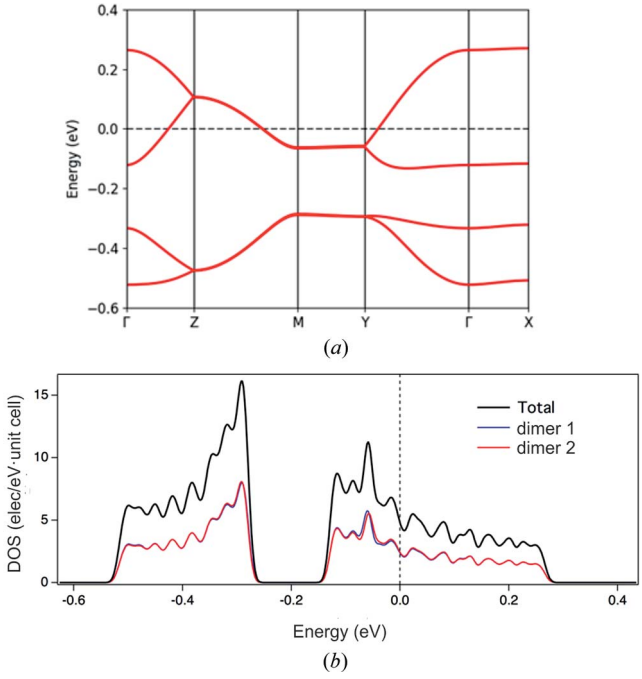

Figure 5
(*a*) Calculated band structure for the 300 K crystal structure of κ-ET-Ag. The energy zero corresponds to the Fermi level. $\Gamma = (0,0,0)$, $X = (\frac{1}{2},0,0)$, $Y = (0,\frac{1}{2},0)$, $Z = (0,0,\frac{1}{2})$ and $M = (0,\frac{1}{2},\frac{1}{2})$ in units of the reciprocal lattice vectors. (*b*) Density of States (DOS) calculated for κ-ET-Ag at 300 K. The black line refers to the total DOS whereas the blue and red lines are the contributions of the two different ET dimers.

4.3. Puzzling physical behaviour

The presence of electric dipoles within the ET dimers has neither been detected by infrared (Sedlmeier *et al.*, 2012) nor by terahertz (Itoh *et al.*, 2013; Dressel *et al.*, 2016) spectroscopy measurements. In particular, the ν_{27} mode, characteristic of the intramolecular vibration and sensitive to its charge, does not present any evidence of a charge disproportionation even at low temperature. Indeed, no splitting has been detected either in κ-ET-Cu or in κ-ET-Ag (Pinterić *et al.*, 2016, 2018; Sedlmeier *et al.*, 2012). This indicates that if there is an intra- or inter-dimer charge disproportionation, it is smaller than the error bar (0.01 e) of spectroscopic determinations. Our structural results are in perfect agreement with this finding. However, they do not explain the dielectric behaviour.

The task is now to explain the dielectric response measured in the Hz–MHz range. Importantly, the experimentally showed absence of sizeable electric dipoles excludes the

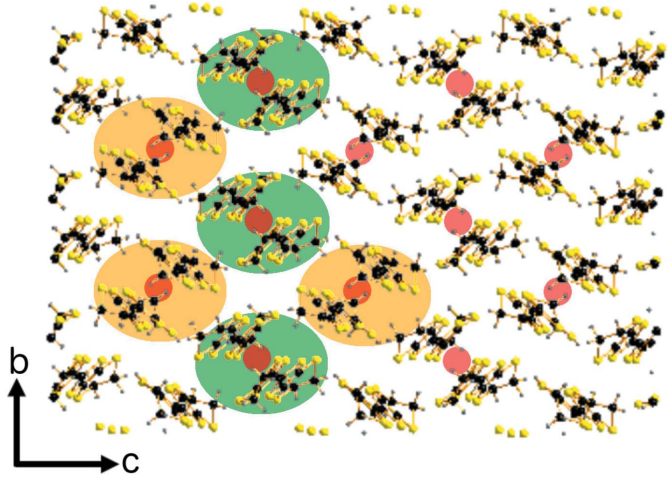

Figure 6
Molecular stack of κ-ET-Ag in the (**bc**) plane showing the charge-rich (orange ellipses) and charge-poor (green ellipses) dimers. The inversion centres remaining in the $P1$ space group are indicated by red circles.

possibility that the dielectric response can be due to their excitation. Therefore, any relevant model of dielectric response should involve the correlated motion of charged domain walls, as previously proposed by Pinterić *et al.* (2014, 2016, 2018), Dressel *et al.* (2016) and in a theoretical work developed by Fukuyama *et al.* (2017). Therefore, the clue lies in identifying random domain structure in κ-ET-Cu and κ-ET-Ag. Such a domain structure can originate in the cyanide groups bridging the polymeric *M*CN chains of the anionic layer which are located at the inversion centres. In the absence of inversion centre, these cyanide groups should be ordered. This order can be achieved in four different domains which are equivalent by the $P2_1/c$ symmetries. The motion of the charged domain walls could induce the observed anomalies in the dielectric response. Interestingly, as pointed out in Section 4.1, the hydrogen bonds between bridging cyanide groups and the ET molecules are shorter in κ-ET-Cu which could additionally favour the ET disorder in κ-ET-Cu more than in κ-ET-Ag. Higher disorder is expected to result in a larger number of domains of smaller size giving rise to a larger in-plane dielectric constant in κ-ET-Cu than in κ-ET-Ag, as observed by Pinterić *et al.* (2014, 2016). Interestingly, hopping conductivity measured in the dc limit also indicates a more effective influence of disorder in the former than in the latter compound (Čulo *et al.*, 2019).

5. Conclusion

Our structural results show that κ-ET-Ag crystallizes in a triclinic space group. The structure known until now (space group $P2_1/c$) is only the average structure. Consequently, due to symmetry arguments, even in the absence of intra-dimer charge disproportionation, an inter-dimer charge disproportionation necessarily occurs. However, our DFT calculations have revealed that such charge disproportionation is very small and of the order of the error bar (0.01 e). The same conclusion is reached from the structural analysis. This result is very similar to that previously reported for κ-ET-Cu (Foury-Leylekian *et al.*, 2018).

However, we found here an important structural difference between κ-ET-Cu and κ-ET-Ag. It concerns the ordering of the terminal ethylene groups in κ-ET-Ag, while these groups are disordered in κ-ET-Cu. This confirms substantial modifications in the hydrogen-bond bonding between the ET layer and the anion layer between these two compounds. However, such structural features have apparently no strong impact on the charge disproportionation because both salts present a charge order of quite weak amplitude.

We have also showed that the charge disproportionation does not evolve with temperature between 300 K and 100 K.

However, the finding of a very small charge disproportionation at ambient pressure does not mean that this quantity should remain small under pressure. If one assumes that the Mott–Hubbard phase present in the κ-ET-*X* (*X* = Cu, Ag) salts is due to intra-dimer charge localization, the enhancement of inter-dimer charge disproportionation under pressure should destabilize the localized state towards a metallic state, a necessary condition to stabilize superconductivity.

It is interesting to notice that the charge disproportionation can evolve under external strain. Lowering the temperature does not provoke a measurable change. But, the pressure or the doping could. From the structural refinement, it seems that the structure of the anion layer, and in particular the effect of the metal anion, is the origin of the breaking of the equivalence of the two dimers. One can enhance the triclinic deformation by shearing of the unit cell and thus increasing the deviation of the alpha angle from 90°. This can be realized by applying an external uniaxial pressure in the diagonal direction, or, alternatively, by a chemical substitution in the anion plane. In this respect it has been recently observed that uniaxial strain destabilizes the Mott-Hubbard phase and induces superconductivity in kappa-ET-Cu and kappa-ET-Ag (Tomeno *et al.*, 2020).

Concerning the spin channel, the triclinic symmetry enables two different dimers and thus at least four different exchange interactions. This complicates the magnetic landscape but can help the emergence of the spin-liquid state as suggested by the dipolar-spin model of reference (Hotta, 2010). It is important to note that the disorder of the terminal ethylene groups is not a prerequisite for the QSL state because κ-ET-Ag with ordered C_2H_4 groups is also a quantum spin liquid. Still, within randomness-induced QSL models (Watanabe *et al.*, 2014; Kawamura& Uematsu, 2019), this disorder, as well as disorder originating from the anionic layer, may support the cooperative action of quantum fluctuations, triangular frustration and dipolar-spin coupling in the stabilization of QSL.

An important question to solve concerns the role of disorder in the anionic layer. Indeed κ-(BEDT-TTF)$_2$Cu[N(CN)$_2$]Cl with a perfectly ordered anionic layer also shows an anomalous dielectric peak. However it does not stabilize a QSL ground state. However, the magnetic frustration is weaker in κ-(BEDT-TTF)$_2$Cu[N(CN)$_2$]Cl. Preliminary X-ray scattering investigation of this system between 300 K and 17 K shows no clear symmetry breaking of the *Pnma* structure commonly used. Further work is required to accurately analyse the structural results obtained for κ-(BEDT-TTF)$_2$Cu[N(CN)$_2$]Cl (Williams *et al.*, 1990) in the light of the present work.

Acknowledgements

We thank Joon I. Jang for his work related to SHG measurements.

Funding information

Work in Spain was supported by MICIU (PGC2018-096955-B-C44 and PGC2018-093863-B-C22), MINECO through the Severo Ochoa (SEV-2015-0496) and Maria de Maeztu (MDM-2017-0767) Programs and Generalitat de Catalunya (2017SGR1506 and 2017SGR1289). Work in Japan is supported by the Japan Society for the Promotion of Science (JSPS) KAKENHI (JP23225005 and JP18H05225).

References

Abdel-Jawad, M., Terasaki, I., Sasaki, T., Yoneyama, N., Kobayashi, N., Uesu, Y. & Hotta, C. (2010). *Phys. Rev. B*, **82**, 125119.

Alemany, P., Pouget, J. P. & Canadell, E. (2015). *J. Phys. Condens. Matter*, **27**, 465702.

Alemany, P., Pouget, J.-P. & Canadell, E. (2012). *Phys. Rev. B*, **85**, 195118.

Artacho, E., Anglada, E., Diéguez, O., Gale, J. D., García, A., Junquera, J., Martin, R. M., Ordejón, P., Pruneda, J. M., Sánchez-Portal, D. & Soler, J. M. (2008). *J. Phys. Condens. Matter*, **20**, 064208.

Artacho, E., Sánchez-Portal, D., Ordejón, P., García, A. & Soler, J. M. (1999). *Phys. Status Solidi B*, **215**, 809–817.

Balents, L. (2010). *Nature*, **464**, 199–208.

Bernu, B., Lhuillier, C. & Pierre, L. (1992). *Phys. Rev. Lett.* **69**, 2590–2593.

Bu, X. & Coppens, P. (1997). *Z. Kristallogr. New Cryst. Struct.* **212**, 103–104.

Čulo, M., Tafra, E., Mihaljević, M., Basletić, M., Kuveždić, M., Ivek, T., Hamzić, A., Tomić, S., Hiramatsu, T., Yoshida, Y., Saito, G., Schlueter, J. A., Dressel, M. & Korin-Hamzić, B. (2019). *Phys. Rev. B*, **99**, 045114.

Dressel, M., Lazić, P., Pustogow, A., Zhukova, E., Gorshunov, B., Schlueter, J. A., Milat, O., Gumhalter, B. & Tomić, S. (2016). *Phys. Rev. B*, **93**, 081201(R).

Foury-Leylekian, P., Ilakovac-Casses, V., Baledent, V., Fertey, P., Arakcheeva, A., Milat, O., Petermann, D., Guillier, G., Miyagawa, K., Kanoda, K., Alemany, P., Canadell, E., Tomic, S. & Pouget, J.-P. (2018). *Crystals*, **8**, 158.

Fukuyama, H., Kishine, J. & Ogata, M. (2017). *J. Phys. Soc. Jpn*, **86**, 123706.

Gallego, S. V., Tasci, E. S., de la Flor, G., Perez-Mato, J. M. & Aroyo, M. I. (2012). *J. Appl. Cryst.* **45**, 1236–1247.

Geiser, U., Wang, H. H., Carlson, K. D., Williams, J. M., Charlier, H. A., Heindl, J. E., Yaconi, G. A., Love, B. J. & Lathrop, M. W. (1991). *Inorg. Chem.* **30**, 2586–2588.

Gomi, H., Ikenaga, M., Hiragi, Y., Segawa, D., Takahashi, A., Inagaki, T. J. & Aihara, M. (2013). *Phys. Rev. B*, **87**, 195126.

Gomi, H., Imai, T., Takahashi, A. & Aihara, M. (2010). *Phys. Rev. B*, **82**, 035101.

Gomi, H., Inagaki, T. J. & Takahashi, A. A. (2016). *Phys. Rev. B*, **93**, 035105.

Groom, C. R., Bruno, I. J., Lightfoot, M. P. & Ward, S. C. (2016). *Acta Cryst.* B**72**, 171–179.

Guionneau, P., Kepert, C. J., Bravic, G., Chasseau, D., Truter, M. R., Kurmoo, M. & Day, P. (1997). *Synth. Met.* **86**, 1973–1974.

Hiramatsu, T., Yoshida, Y., Saito, G., Otsuka, A., Yamochi, H., Maesato, M., Shimizu, Y., Ito, H. & Kishida, H. (2015). *J. Mater. Chem. C*, **3**, 1378–1388.

Hiramatsu, T., Yoshida, Y., Saito, G., Otsuka, A., Yamochi, H., Maesato, M., Shimizu, Y., Ito, H., Nakamura, Y., Kishida, H., Watanabe, M. & Kumai, R. (2017). *Bull. Chem. Soc. Jpn*, **90**, 1073–1082.

Hohenberg, P. & Kohn, W. (1964). *Phys. Rev.* **136**, B864.

Hotta, C. (2010). *Phys. Rev. B*, **82**, 241104.

Ilakovac, V., Carniato, S., Foury-Leylekian, P., Tomić, S., Pouget, J.-P., Lazić, P., Joly, Y., Miyagawa, K., Kanoda, K. & Nicolaou, A. (2017). *Phys. Rev. B*, **96**, 184303.

Itoh, K., Itoh, H., Naka, M., Saito, S., Hosako, I., Yoneyama, N., Ishihara, S., Sasaki, T. & Iwai, S. (2013). *Phys. Rev. Lett.* **110**, 106401.

Jeschke, H. O., de Souza, M., Valentí, R., Manna, R. S., Lang, M. & Schlueter, J. A. (2012). *Phys. Rev. B*, **85**, 035125.

Kandpal, H. C., Opahle, I., Zhang, Y.-Z., Jeschke, H. O. & Valentí, R. (2009). *Phys. Rev. Lett.* **103**, 067004.

Kanoda, K. & Kato, R. (2011). *Annu. Rev. Condens. Matter Phys.* **2**, 167.

Kawamura, H. & Uematsu, K. (2019). *J. Phys. Condens. Matter*, **31**, 504003.

Kleinman, L. & Bylander, D. M. (1982). *Phys. Rev. Lett.* **48**, 1425.

Kohn, W. & Sham, L. J. (1965). *Phys. Rev.* **140**, A1133.

Komatsu, T., Matsukawa, N., Inoue, T. & Saito, G. (1996). *J. Phys. Soc. Jpn*, **65**, 1340–1354.

Koretsune, T. & Hotta, C. (2014). *Phys. Rev. B*, **89**, 045102.

Kurosaki, Y., Shimizu, Y., Miyagawa, K., Kanoda, K. & Saito, G. (2005). *Phys. Rev. Lett.* **95**, 177001.

Li, H., Clay, R. T. & Mazumdar, S. (2010). *J. Phys. Condens. Matter*, **22**, 272201.

Manna, R. S., de Souza, M., Brühl, A., Schlueter, J. A. & Lang, M. (2010). *Phys. Rev. Lett.* **104**, 016403.

Matsubara, T. & Kotani, A. (1984). Editors. *Superconductivity in Magnetic and Exotic Materials*. Berlin: Springer.

Miyamoto, T. (2019). Private communication.

Monkhorst, H. J. & Pack, J. D. (1976). *Phys. Rev. B*, **13**, 5188.

Naka, M. & Ishihara, S. (2010). *J. Phys. Soc. Jpn*, **79**, 063707.

Naka, M. & Ishihara, S. (2013). *J. Phys. Soc. Jpn.* **82**, 023701.

Nakamura, K., Yoshimoto, Y., Kosugi, T., Arita, R. & Imada, M. (2009). *J. Phys. Soc. Jpn*, **78**, 083710.

Nakamura, Y., Hiramatsu, T., Yoshida, Y., Saito, G. & Kishida, H. (2017). *J. Phys. Soc. Jpn*, **86**, 014710.

Nakamura, Y., Yoneyama, N., Sasaki, T., Tohyama, T., Nakamura, A. & Kishida, H. (2014). *J. Phys. Soc. Jpn*, **83**, 074708.

Papavassiliou, A., Lagouvardos, G. C., Terzis, A., Amiell, J., Garrigou-Lagrange, C., Delhaès, P., Hilti, B. & Pfeiffer, J. (1993). *Synth. Met.* **61**, 267–273.

Perdew, J. P., Burke, K. & Ernzerhof, M. (1996). *Phys. Rev. Lett.* **77**, 3865.

Petříček, V., Dušek, M. & Palatinus, L. (2014). *Z. Kristallogr.* **229**, 345–352.

Pinterić, M., Čulo, M., Milat, O., Basletić, M., Korin-Hamzić, B., Tafra, E., Hamzić, A., Ivek, T., Peterseim, T., Miyagawa, K., Kanoda, K., Schlueter, J. A., Dressel, M. & Tomić, S. (2014). *Phys. Rev. B*, **90**, 195139.

Pinterić, M., Lazić, P., Pustogow, A., Ivek, T., Kuveždić, M., Milat, O., Gumhalter, B., Baslestić, M., Čulo, M., Korin-Hamzić, B., Löhle, A., Hübner, R., Sanz Alonso, M., Hiramatsu, T., Yoshida, Y., Saito, G., Dressel, M. & Tomić, S. (2016). *Phys. Rev. B*, **94**, 161105(R).

Pinterić, M., Rivas Góngora, D., Rapljenovic, Z., Ivek, T., Čulo, M., Korin-Hamzic, B., Milat, O., Gumhalter, B., Lazic, P., Sanz Alonso, M., Li, W., Pustogow, A., Gorgen Lesseux, G., Dressel, M. & Tomic, S. (2018). *Crystals*, **8**, 190.

Poirier, M., de Lafontaine, M., Miyagawa, K., Kanoda, K. & Shimizu, Y. (2014). *Phys. Rev. B*, **89**, 045138.

Pouget, J.-P., Alemany, P. & Canadell, E. (2018). *Mater. Horizons*, **5**, 590–640.

Powell, B. J. & McKenzie, R. H. (2011). *Rep. Prog. Phys.* **74**, 056501.

Pustogow, A., Bories, M., Löhle, A., Rösslhuber, R., Zhukova, E., Gorshunov, B., Tomić, S., Schlueter, J.A., Hübner, R., Hiramatsu, T. Toshida, Y., Saito, G., Kato R., Lee, T.-H., Dobrosavljević, V., Fratini, S. & Dressel, M. (2018). *Nat. Mater.* **17**, 773–777.

Rigaku Oxford Diffraction (2015). *CrysAlis PRO*. Rigaku Oxford Diffraction, Yarnton, England.

Sedlmeier, K., Elsässer, S., Neubauer, D., Beyer, R., Wu, D., Ivek, T., Tomić, S., Schlueter, J. A. & Dressel, M. (2012). *Phys. Rev. B*, **86**, 245103.

Seo, H., Merino, J., Yoshioka, H. & Ogata, M. (2006). *J. Phys. Soc. Jpn*, **75**, 051009.

Shimizu, Y., Hiramatsu, T., Maesato, M., Otsuka, A., Yamochi, H., Ono, A., Itoh, M., Yoshida, M., Takigawa, M., Yoshida, Y. & Saito, G. (2016). *Phys. Rev. Lett.* **117**, 107203.

Shimizu, Y., Miyagawa, K., Kanoda, K., Maesato, M. & Saito, G. (2003). *Phys. Rev. Lett.* **91**, 107001.

Souza, M. de, Brühl, A., Müller, J., Foury-Leylekian, P., Moradpour, A., Pouget, J.-P. & Lang, M. (2009). *Phys. B Condens. Matter*, **404**, 494–498.

Tomeno, S., Maesato, M., Yoshida, Y., Hiramatsu, T., Saito, G. & Kitagawa, H. (2020). *J. Phys. Soc. Jpn*, **89**, 054709.
Tomić, S. & Dressel, M. (2015). *Rep. Prog. Phys.* **78**, 096501.
Troullier, N. & Martins, J. L. (1991). *Phys. Rev. B*, **43**, 1993–2006.
Watanabe, K., Kawamura, H., Nakano, H. & Sakai, T. (2014). *J. Phys. Soc. Jpn*, **83**, 034714.
Williams, J. M., Kini, A. M., Wang, H. H., Carlson, K. D., Geiser, U., Montgomery, L.K., Pyrka, G. J., Watkins, D. M., Kommers, J. M., Boryschuk, S. J., Strieby Crouch, A. V., Kwok, W. K., Schirber, J. E., Overmyer, D. L, Jung, D. & Whangbo, M.-H. (1990). *Inorg. Chem.* **29**, 3262–3274
Yamashita, S., Nakazawa, Y., Oguni, M., Oshima, Y., Nojiri, H., Shimizu, Y., Miyagawa, K. & Kanoda, K. (2008). *Nat. Phys.* **4**, 459–462.
Yamochi, H., Nakamura, T., Komatso, T., Matsukawa, N., Inoue, T., Saito, G., Mori, T., Kusunoki, M. & Sakaguchi, K. (1992). *Solid State Commun.* **82**, 101–105.